# *Supporting Information*

## Interfacially coupled Ni with Fe-N doped carbon as a potential electrocatalyst for overall alkaline seawater splitting

Sriram Sundarraj*[a], Giddaerappa[a], P. Abdul Junaid[a], P. Sana[a], Vishnu Bakthavachalam[b], and K. Sudhakara Prasad*[a]

[a]*Nano Material Research Laboratory (NMRL), Smart Materials and Devices, Yenepoya Research Centre, Yenepoya (Deemed to be University), Deralakatte, Mangalore 575 018, India.*

[b]*Chemical Engineering Division, BRIC National Agri-Food and Biomanufacturing Institute (Formerly, Center of Innovative and Applied Bioprocessing), Mohali, Punjab 140306, India*

Total Pages: 41

Total Figures: 23

Total Tables: 11

## 1. Experimental section

### 1.1 Materials and methods

Pyrrole, nickel(II) chloride hexahydrate, Potassium hydroxide, Iron chloride Hexahydrate, and isopropanol were purchased from Sigma-Aldrich chemicals and double-distilled DI water. Sea water is collected from the Someshwar beach and used directly in the reaction without any further purification. Nickel foam (thickness: 0.5 mm) was purchased from Vritra Technologies, Delhi, India. These chemicals were used as received without further purification. Deionized (DI) water, ethanol, and 3 M HCl were used as solvents and for washing.

### 1.2 Synthesis of $NiFe_2O_4/NiO/Fe_2O_3$ embedded with N-doped carbon

The $NiFe_2O_4/NiO/Fe_2O_3$ embedded with N-doped carbon was synthesized by a mechanochemical process using a motor and pestle. For the polymerization of pyrrole under solvent-free conditions, $FeCl_3.6H_2O$ was employed as both oxidant and dopant. About 500 µL of pyrrole, 0.5 g of $FeCl_3.6H_2O$, and different weight ratios of nickel chloride were added into the reaction (1 g, 1.2 g, 1.4 g) was subjected to grinding for 15 mins, and a black-colored powder was formed. Then the mixture was pyrolysis in a muffle furnace for 3 h at 500 ˚C, and it was named N@C-$Ni_1$-$Fe_{0.5}$, N@C-$Ni_{1.2}$-$Fe_{0.5}$, N@C-$Ni_{1.4}$-$Fe_{0.5}$, respectively. And also, for electrochemical comparison, control electrocatalyst were synthesised with the same active electrocatalyst without nickel (N@C-$Fe_2O_3$), without nitrogen doped carbon (Ni-Fe oxide) and without calcination polypyrrole (PPY), catalysts were synthesized.

### 1.3 Physical characterization

X-ray diffraction (XRD) and Fourier transform infrared (FTIR) spectra of electrocatalysts were recorded with Thermo XRD Equinox 1000 and Shimadzu IR Tracer-100. The morphology, elemental mapping, and EDX of N@C-$Ni_{1.2}$-$Fe_{0.5}$ were determined by using a *ZEISS* Sigma 300 field emission scanning electron microscope (FESEM). JEM-2100 Plus

was used to record transmission electron microscope (TEM) analysis of the N@C-$Ni_{1.2}$-$Fe_{0.5,}$ and the selected area electron diffraction (SAED) pattern was taken from JEOL JEM-2100 Plus. The elemental composition of N@C-$Ni_{1.2}$-$Fe_{0.5}$ was analyzed by XPS (X-ray photoelectron spectroscopy) with a K-ALPHA SURFACE ANALYSIS spectrometer. For fitting the XPS spectrum, XPSPEAK41 fitting software was used for XPS fitting.

**1.4 Electrocatalytic characterization**

The catalytic performances of the electrodes for water splitting were studied using a CHI 708E electrochemical workstation and operated at room temperature. The Nickel foam (NF) was used as a working electrode for the electrochemical analysis. The Ag/AgCl (3 M KCl) electrode (RHE conversion: $E(RHE) = E_{Ag/AgCl} + E^{o}_{Ag/AgCl} + 0.059pH$) and Pt wire were used as the reference and counter electrodes. To remove the surface oxidized layer, a piece of Ni foam (0.5 cm × 0.5 cm) was cleaned through sonication consecutively in 3 M HCl, ethanol, and DI water (5 min each) and dried before using as a substrate. The slurry was prepared by mixing 5 mg of the catalyst with 490 µl of isopropanol in the presence of 10 µl Nafion (5 wt %). And it was sonicated for 20 min. in an ultrasonicator. The commercially available noble catalysts ($IrO_2$, $RuO_2$ & Pt/C) and bare NF were used for comparison. About 5 mg of commercial $IrO_2$, $RuO_2$ & Pt/C suspension was prepared by following a similar methodology, and bare NF. All measurements were carried out in 1 M KOH (aq). Electrocatalysts OER and HER properties have been analyzed using polarization curves, cyclic voltammetry, electrochemical impedance spectroscopy (EIS), and chronopotentiometry. The OER and HER activity of the catalyst has been measured by linear sweep voltammetry (LSV) on the NF electrode (scan rate: 10 mV $s^{-1}$). The charge transfer co-efficient (α) was calculated by $\alpha=2.303RT/nF\cdot b$ [R = Universal gas constant (8.314 J $mol^{-1}K^{-1}$), T = Temperature in Kelvin (typically 298 K at room temperature), n = Number of electrons transferred in the rate-determining reaction, F = Faraday's constant (96,485 C $mol^{-1}$), and b = Tafel slope (V/decade)].

Here, the turnover frequency (TOF) rate of evolved molecular $O_2$ per surface active site per second can be calculated. TOF = $\frac{JA}{4f\,n}$ where J- Current density (mA $cm^{-2}$), A- Area, n - number of electrons required to produce 1 $O_2/H_2$ molecule, F- Faraday's constant (96,485 C $mol^{-1}$), n - number of moles of metal active species in the catalyst. TO determine the TOF for OER, it was calculated from the potential 1.6 V and HER, it was -0.1 V. To calculate the ECSA, we used the following equation: ECSA = $C_{dl}/C_s$ [$C_{dl}$ - double-layer capacitance (mF $cm^{-2}$), Cs - specific capacitance]. The Cs value represents the smooth plane capacitance on a metal surface in a 1.0 M KOH solution of 0.04 mF $cm^{-2}$. [1] The roughness factor (RF) (RF = ECSA/GSA) for electrocatalysts has been calculated [GSA - geometric surface area (0.25 $cm^2$)]. The ECSA-normalized LSV was calculated using the ECSA value. The impedance of the electrocatalyst was measured by electrochemical impedance spectroscopy (EIS) over a frequency range of 100 kHz to 10 mHz with a sinusoidal perturbation amplitude of 0.5V. To evaluate the electrochemical performance in glassy carbon electrode (GC: electrode surface area - 0.0706 $cm^{-2}$), the electrode was polished with alumina slurry, and 5 mg of electrocatalyst was added with 485 µl of isopropanol and 15 µl of Nafion. The slurry was sonicated for 30 min, and the ink was drop-cast onto the GC electrode surface. The experiments were carried out in 1 M KOH.

**1.5. Colorimetric chlorine conformation test.**

To determine the conformation of oxidizing chlorine species generated during seawater oxidation was qualitatively examined using a starch-iodine colorimetric method with commercially available test paper. After long-term stability, 200 µL of electrolyte was collected from the vicinity of the working electrode and drop-cast onto the testing paper to confirm the presence of oxidized chlorine. To check the rationality of the colorimetric analysis, 200µl of 0.5 mM NaClO solution was used as a positive control solution for colorimetric analysis.

**Figure S1. XRD spectrum of N@C-$Ni_{1.2}$-$Fe_{0.5}$.**

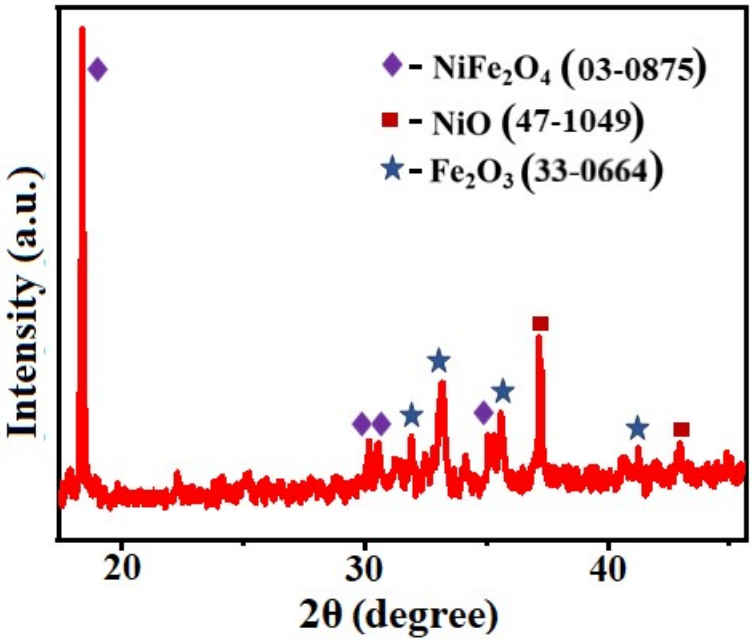

**Figure S2. BET pore size distribution of N@C-$Ni_1$-$Fe_{0.5}$, N@C-Ni1.2-Fe0.5, and N@C-$Ni_{1.4}$-$Fe_{0.5}$.**

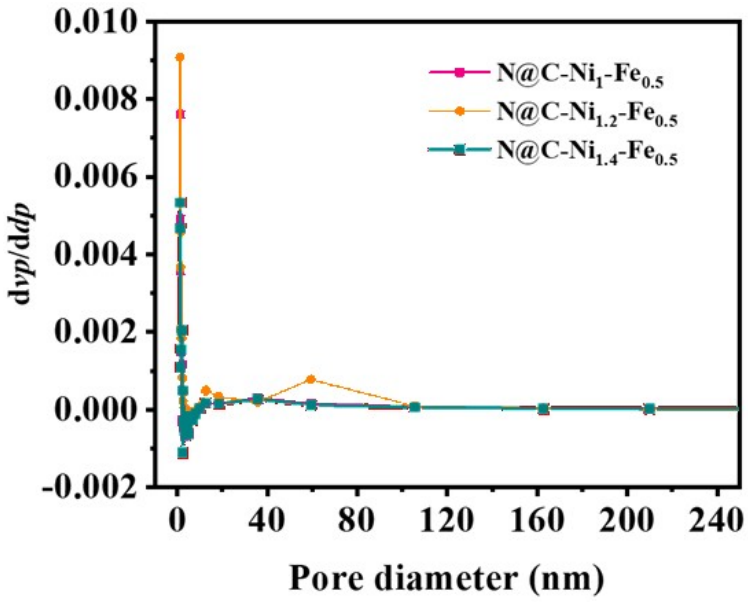

**Figure S3. FTIR spectra of PPY, N@C-$Fe_2O_3$, and different ratios of Ni composites (N@C-Ni-Fe's).**

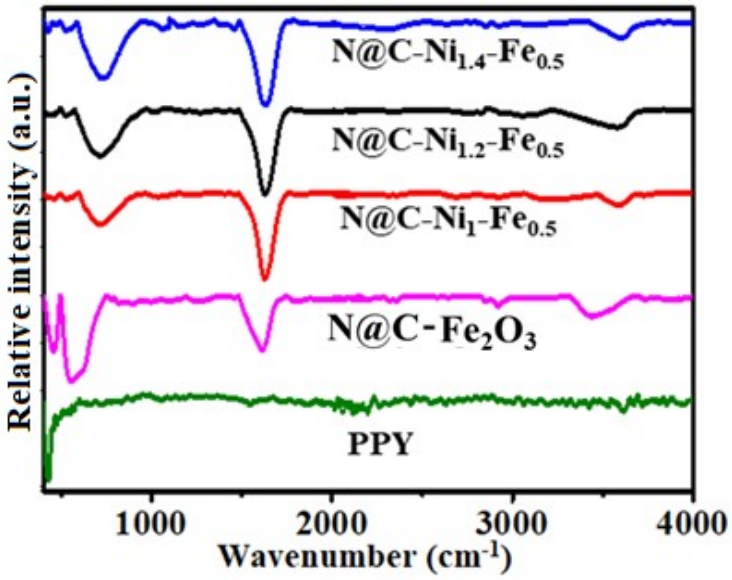

**Figure S4. Elemental mapping and EDAX spectra of N@C-$Fe_2O_3$.**

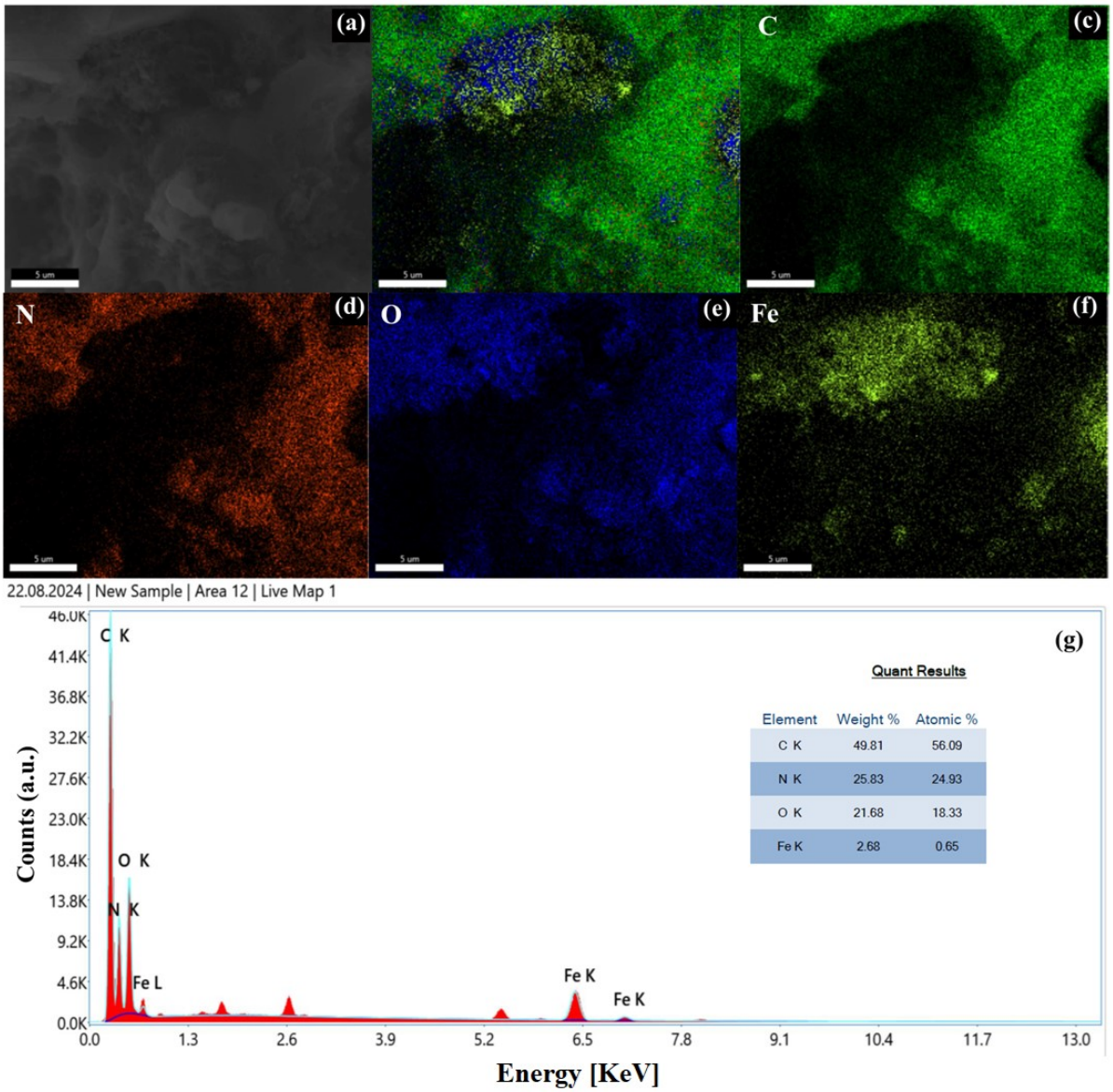

**Figure S5. Elemental mapping and EDAX spectra of N@C-$Ni_{1.2}$-$Fe_{0.5}$**

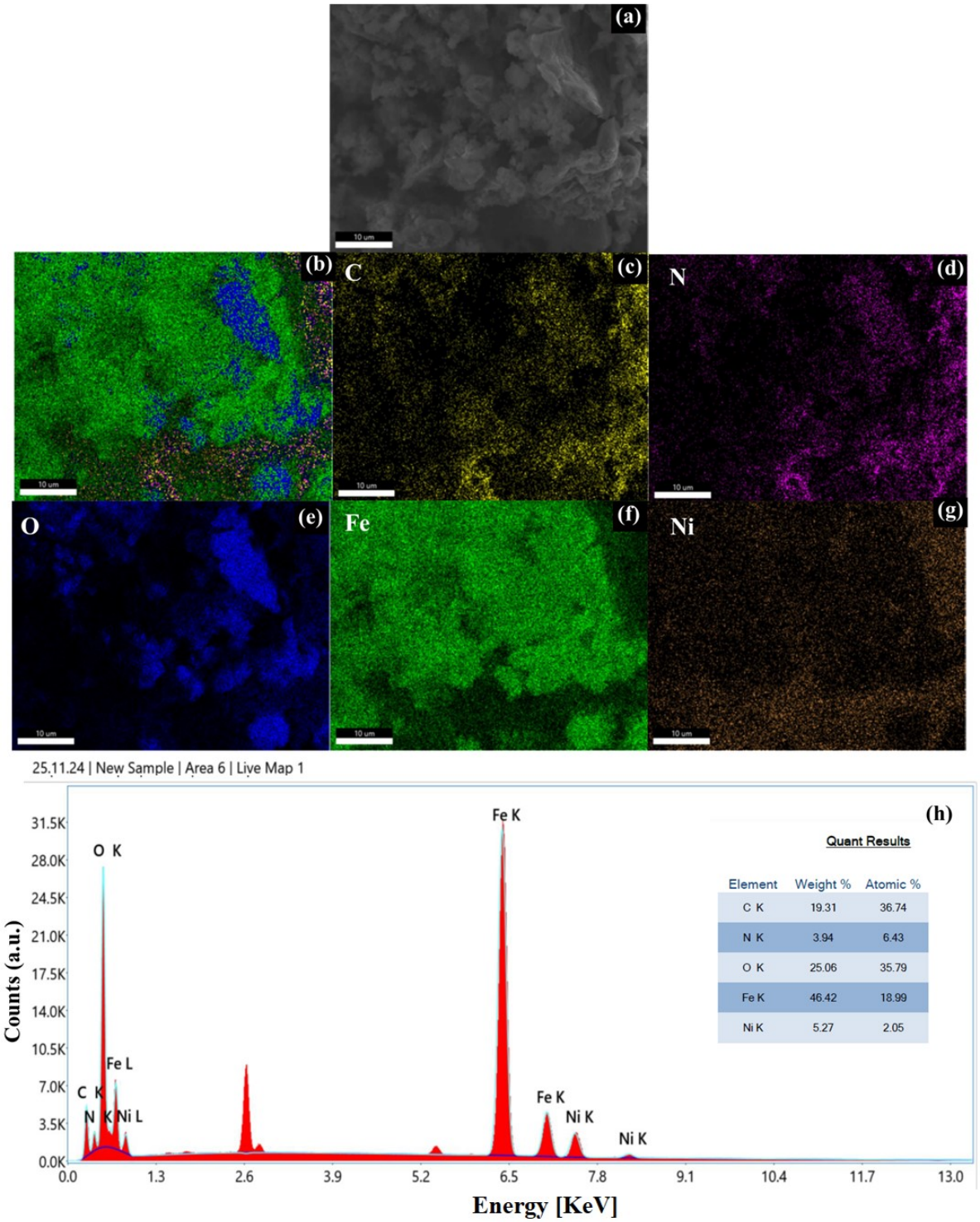

**Figure S6. (a) LSV curves of N@C-$Ni_{1.2}$-$Fe_{0.5}$, Ni-Fe oxide, and NF, and (b) LSV curves of N@C-$Ni_{1.2}$-$Fe_{0.5}$, $IrO_2$, and GC, (c) Oxidation of peak of N@C-$Ni_{1.2}$-$Fe_{0.5}$ and bare GC during OER, and (d) Tafel slope of the synthesized electrocatalyst.**

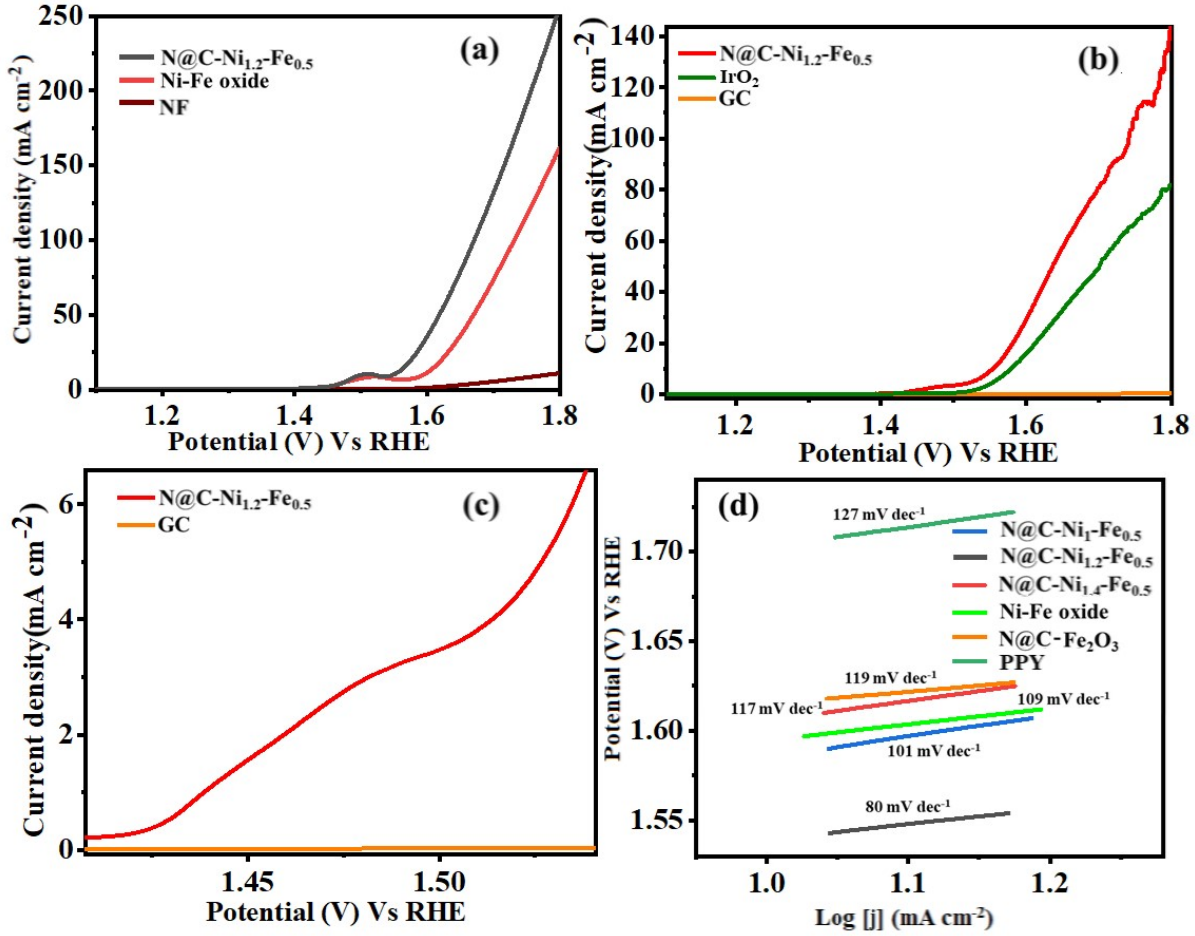

**Figure S7. Post OER XRD spectra of N@C-$Ni_{1.2}$-$Fe_{0.5}$**

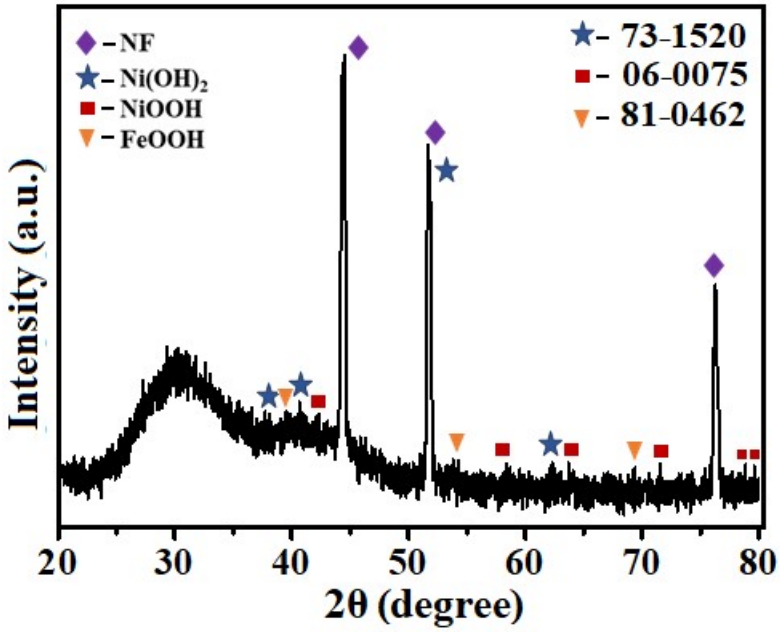


**Figure S8. Post OER FESEM of N@C-$Ni_{1.2}$-$Fe_{0.5}$**

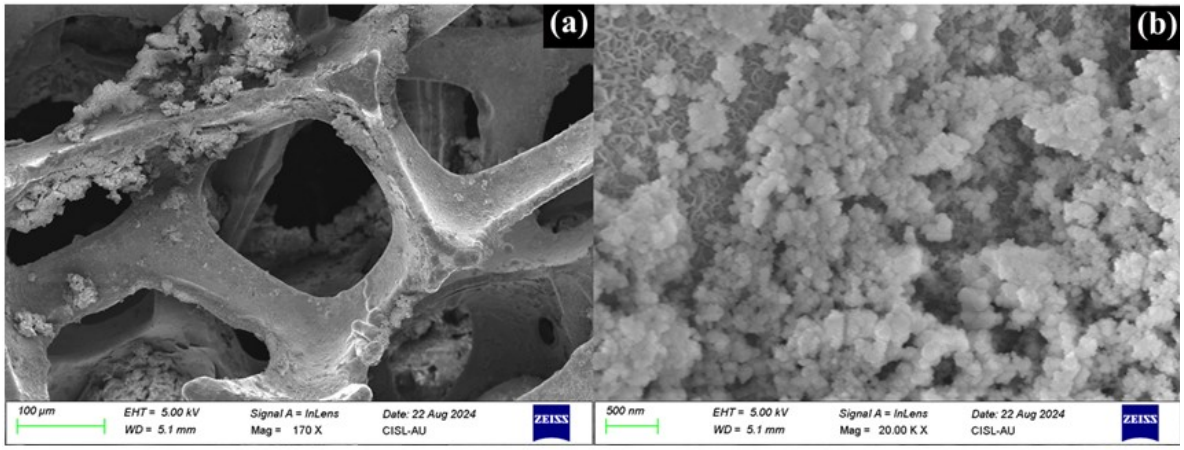

**Figure S9. Post OER elemental mapping and EDX spectra of N@C-$Ni_{1.2}$-$Fe_{0.5}$**

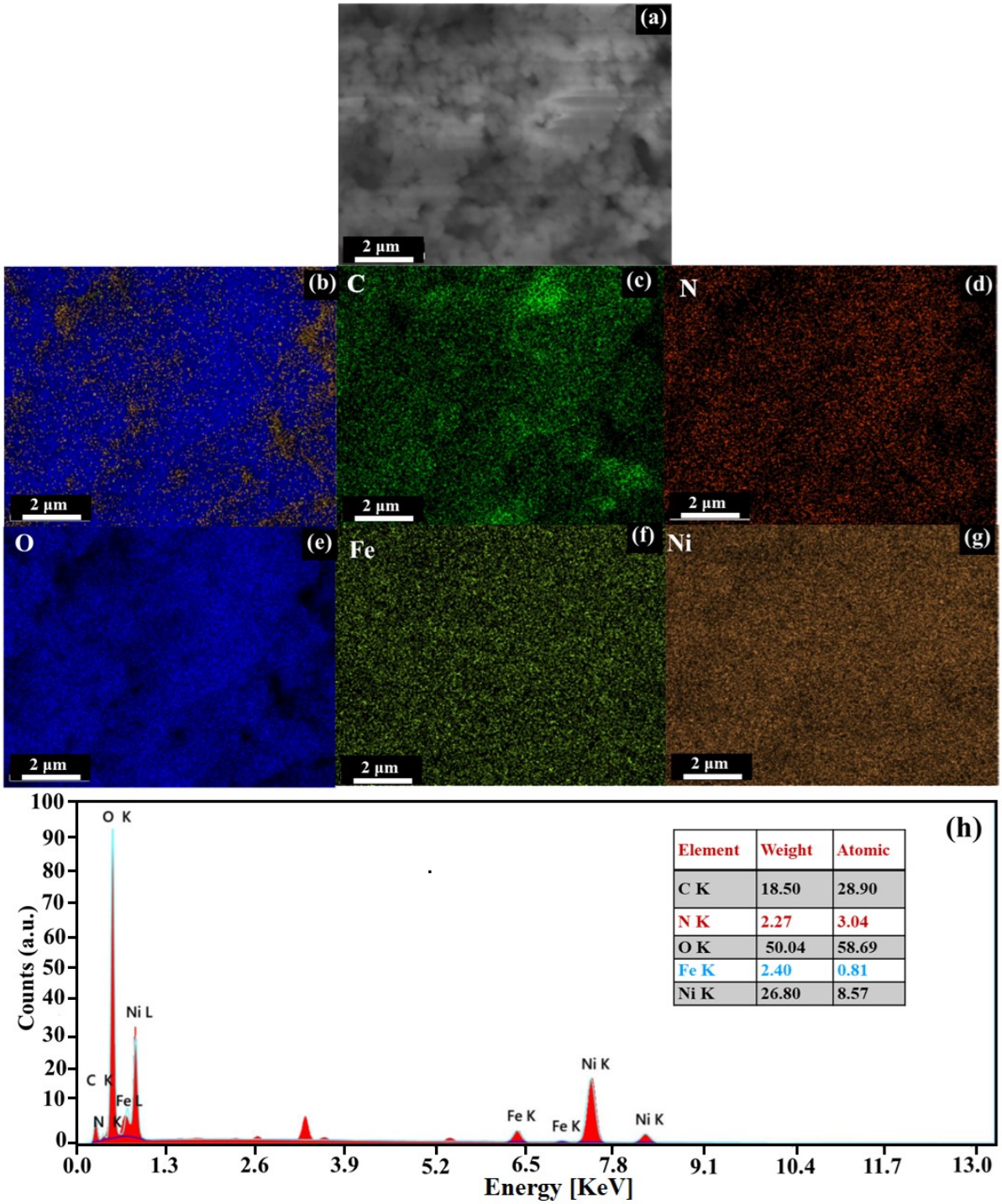


| Element | Weight | Atomic |
|---|---|---|
| C K | 18.50 | 28.90 |
| N K | 2.27 | 3.04 |
| O K | 50.04 | 58.69 |
| Fe K | 2.40 | 0.81 |
| Ni K | 26.80 | 8.57 |

**Figure S10. Post OER XPS spectra of N@C-$Ni_{1.2}$-$Fe_{0.5}$**

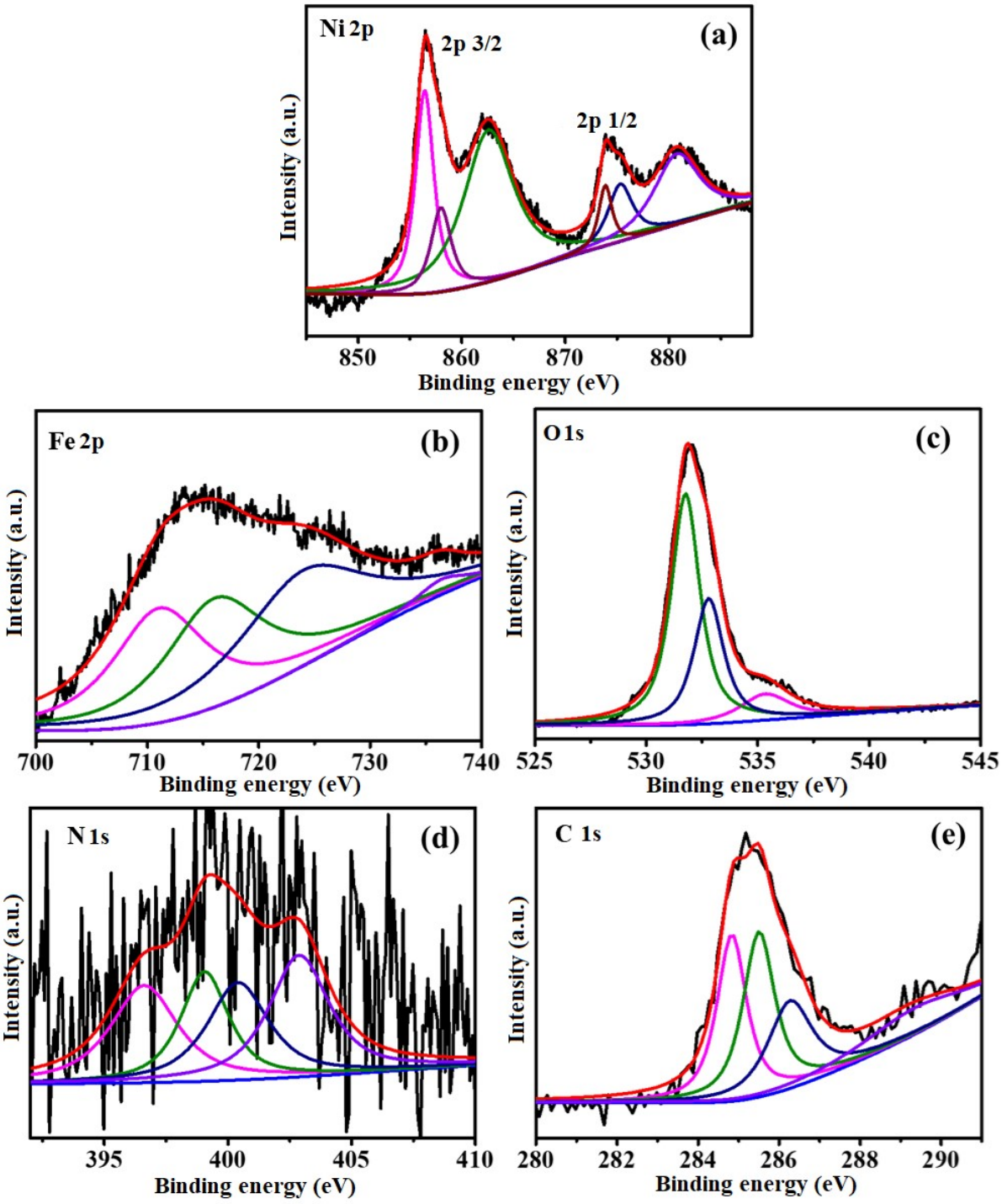

**Figure S11. HER LSV curves of N@C-$Ni_{1.2}$-$Fe_{0.5}$, Pt/C, and GC.**

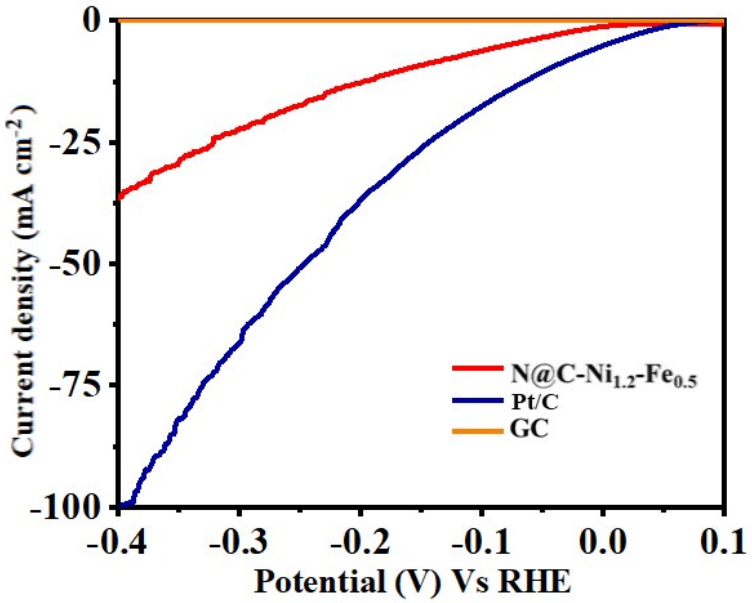

**Figure S12. Post HER XRD spectra of N@C-$Ni_{1.2}$-$Fe_{0.5}$**

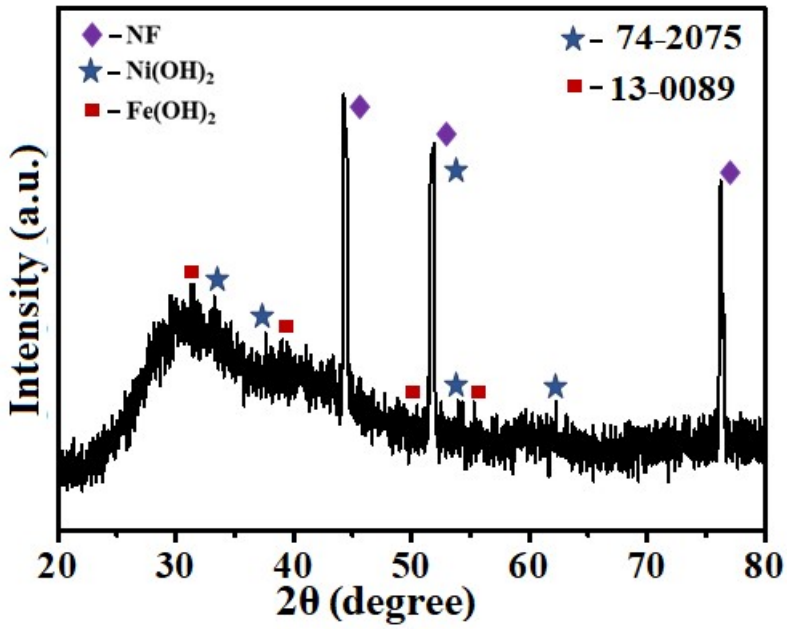

**Figure S13. Post HER FESEM of N@C-$Ni_{1.2}$-$Fe_{0.5}$**

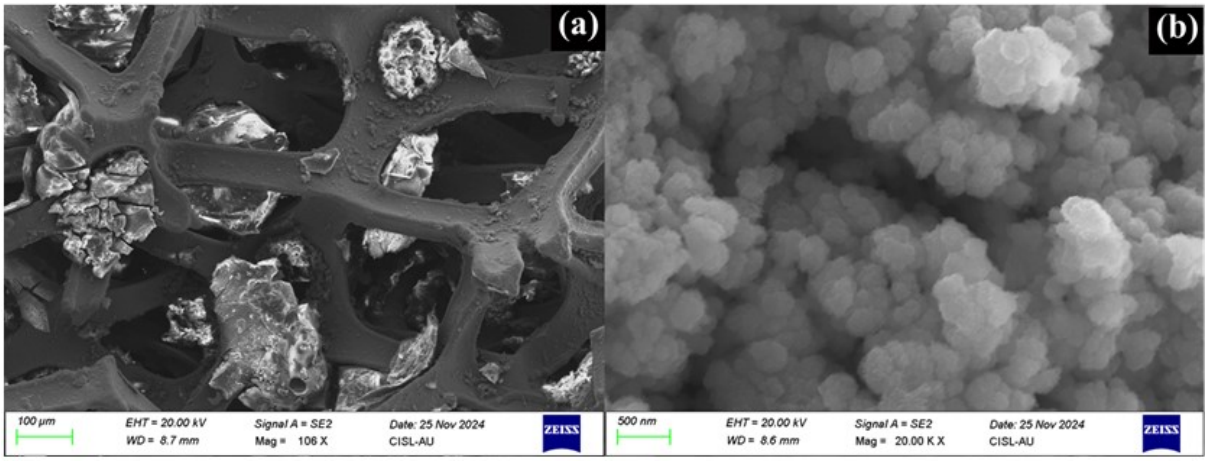

**Figure S14. Post HER elemental mapping and EDX spectra of N@C-$Ni_{1.2}$-$Fe_{0.5}$**

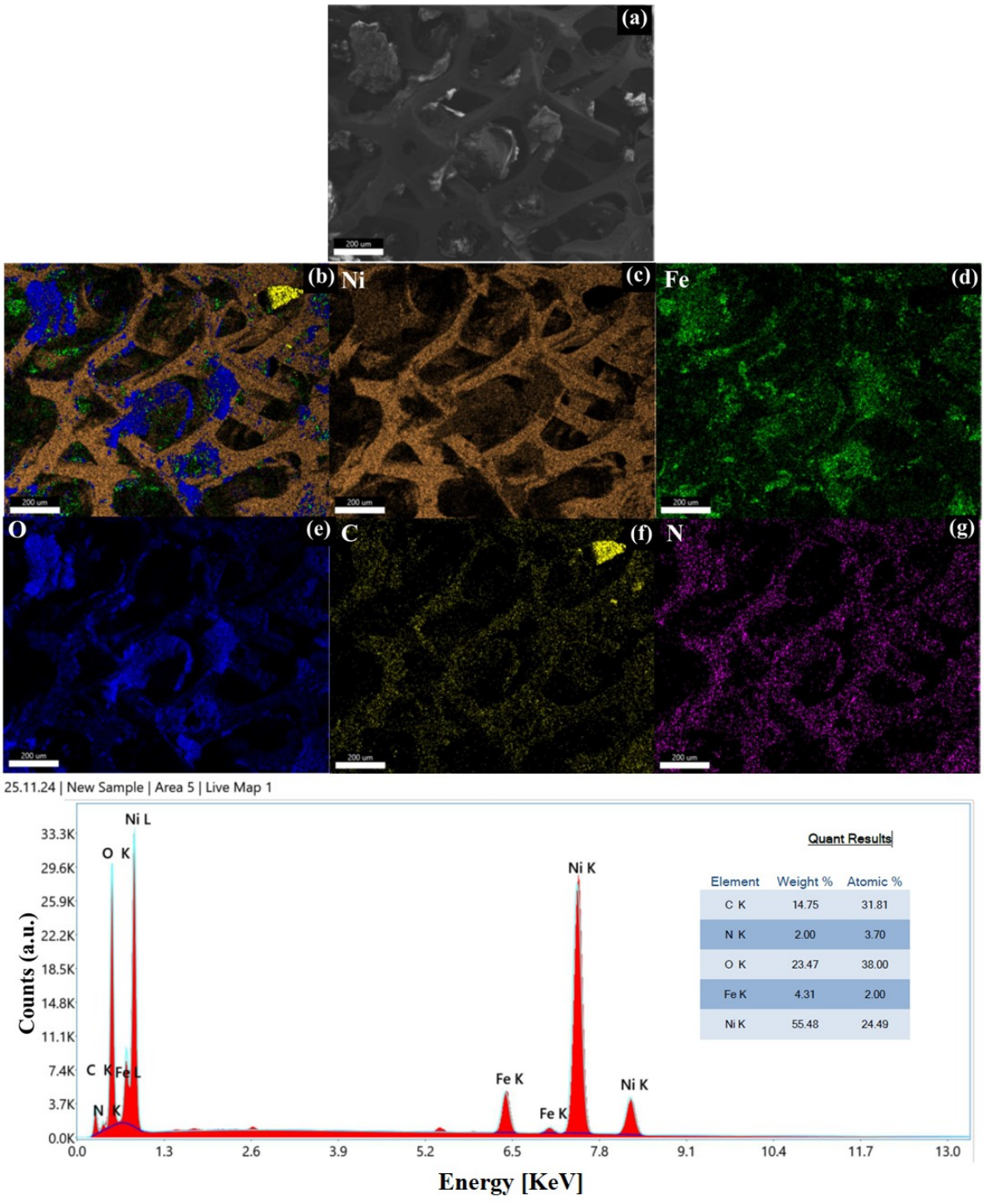

**Figure S15. Post HER XPS spectra of N@C-$Ni_{1.2}$-$Fe_{0.5}$**

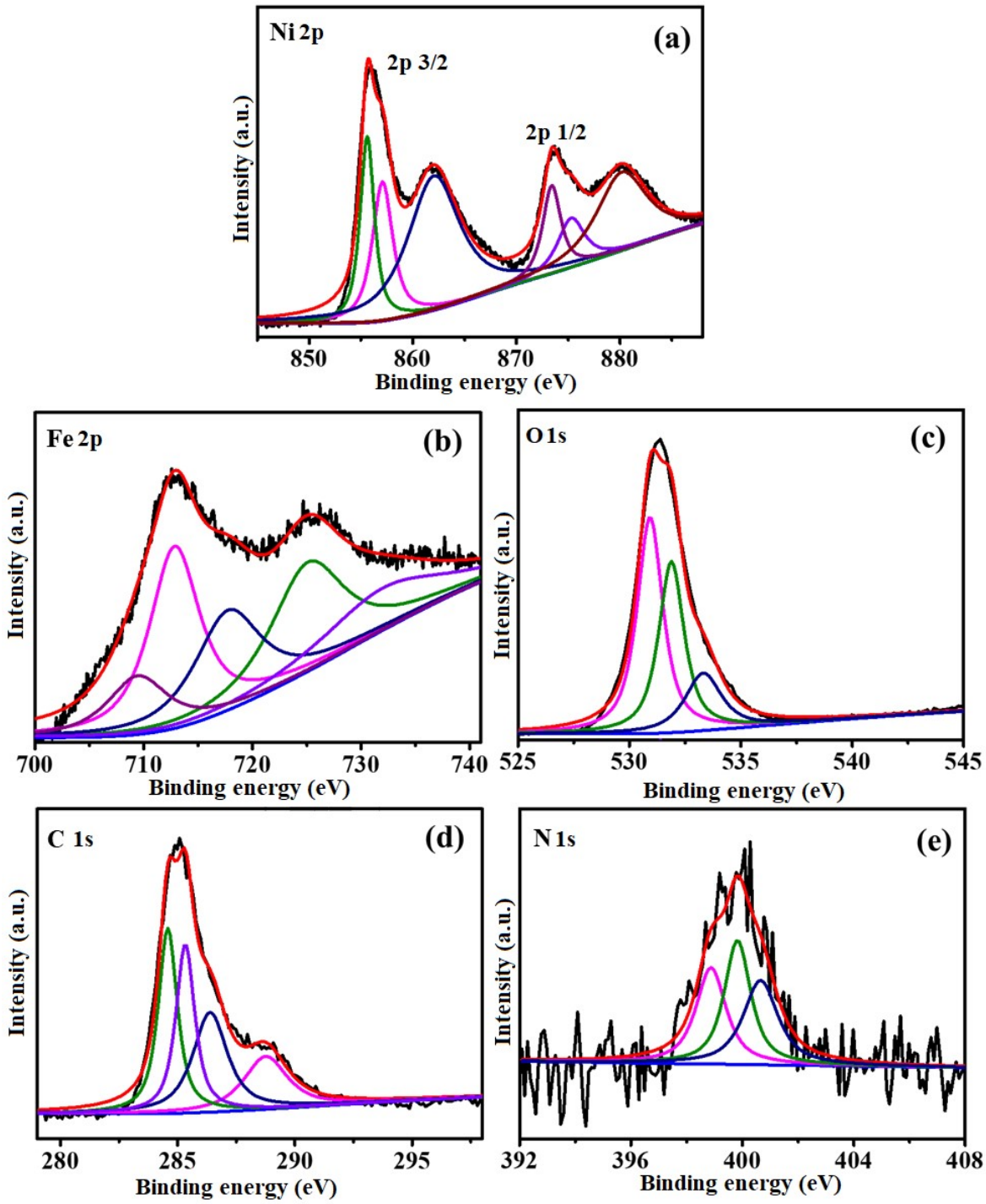

**Figure S16. (a, c & e) ECSA curve of N@C-$Ni_1$-$Fe_{0.5}$, N@C-$Ni_{1.2}$-$Fe_{0.5}$, and N@C-$Ni_{1.4}$-$Fe_{0.5}$ at different scan rates; and (b d, & f) Cdl of N@C-$Ni_1$-$Fe_{0.5}$, N@C-$Ni_{1.2}$-$Fe_{0.5}$, and N@C-$Ni_{1.4}$-$Fe_{0.5}$.**

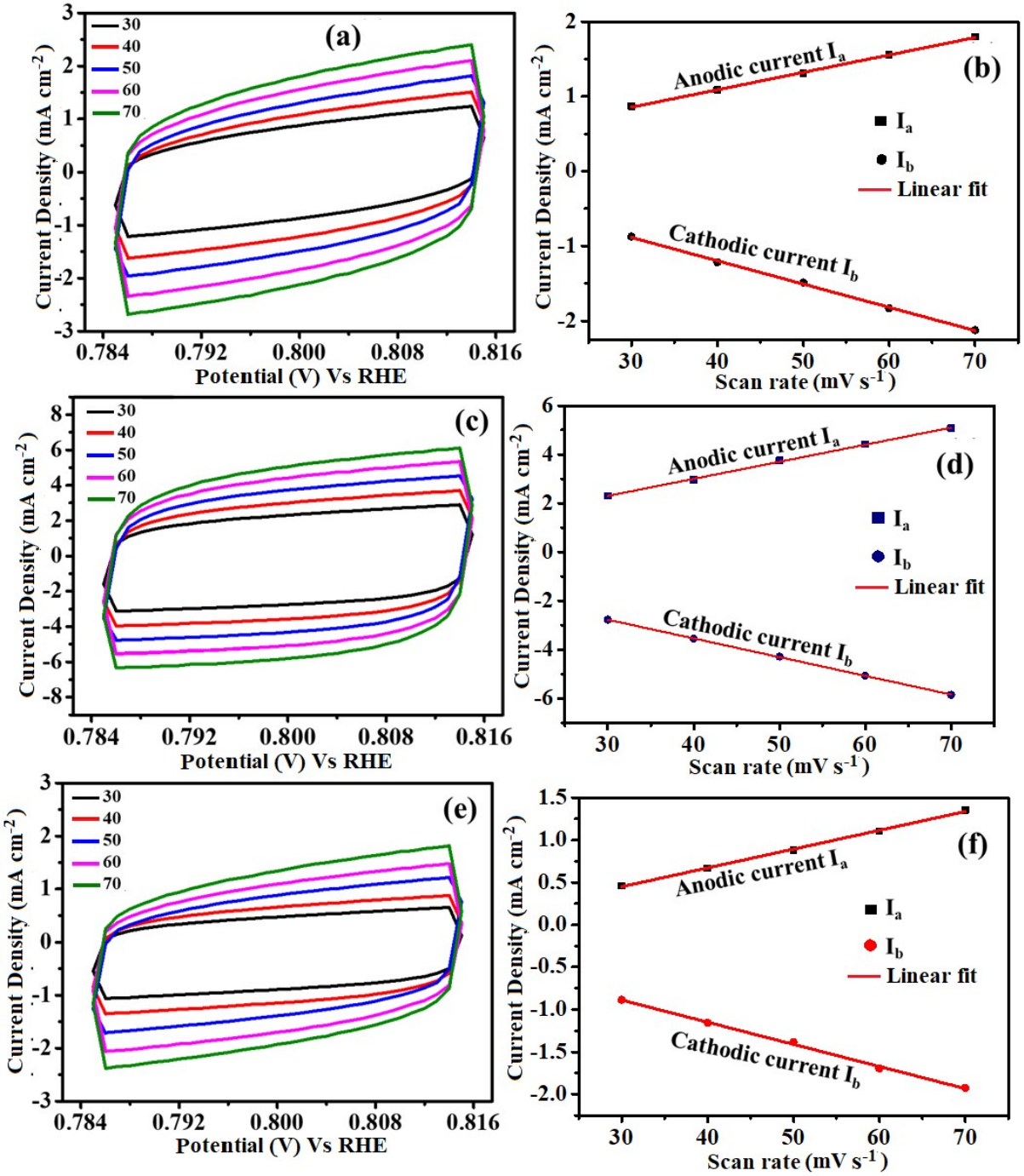

**Figure S17. ECSA normalized LSV of N@C-$Ni_{1.2}$-$Fe_{0.5}$ in 1 M KOH.**

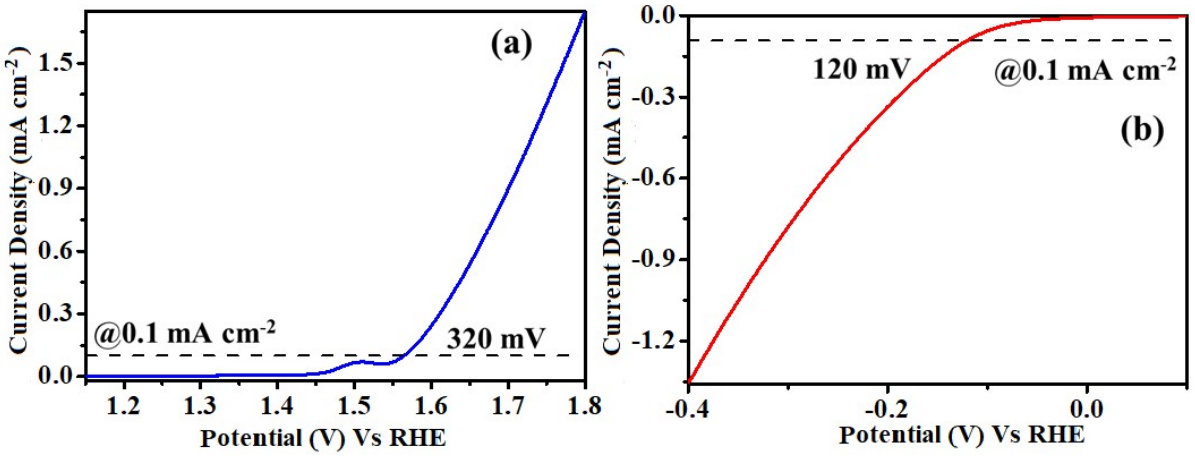

**Figure S18. Chronopotentiometry of full cell; (a) N@C-$Ni_{1.2}$-$Fe_{0.5}$ and (b) Ni-Fe oxide in 1 M KOH**

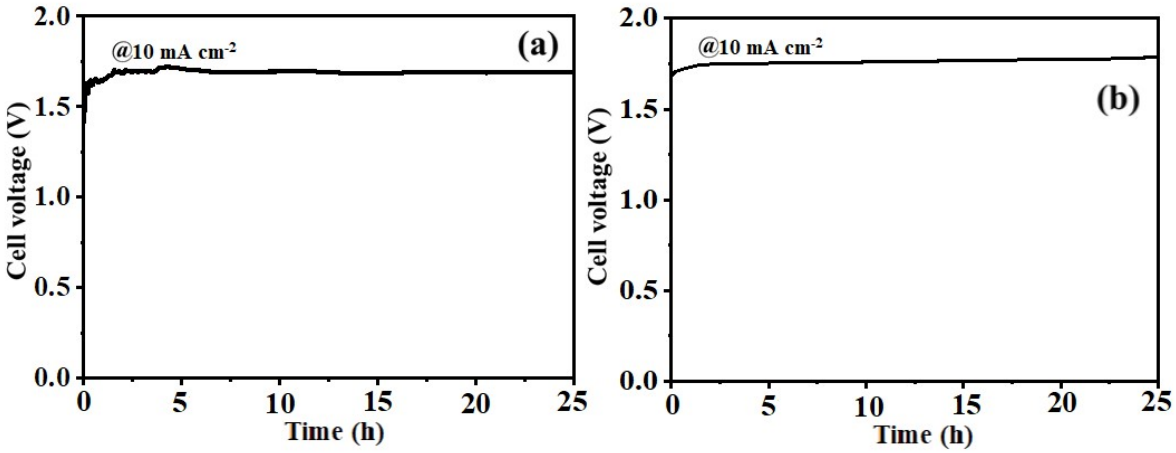

**Figure S19. OER chronopotentiometry of N@C-$Ni_{1.2}$-$Fe_{0.5}$ in 1 M KOH + natural seawater**

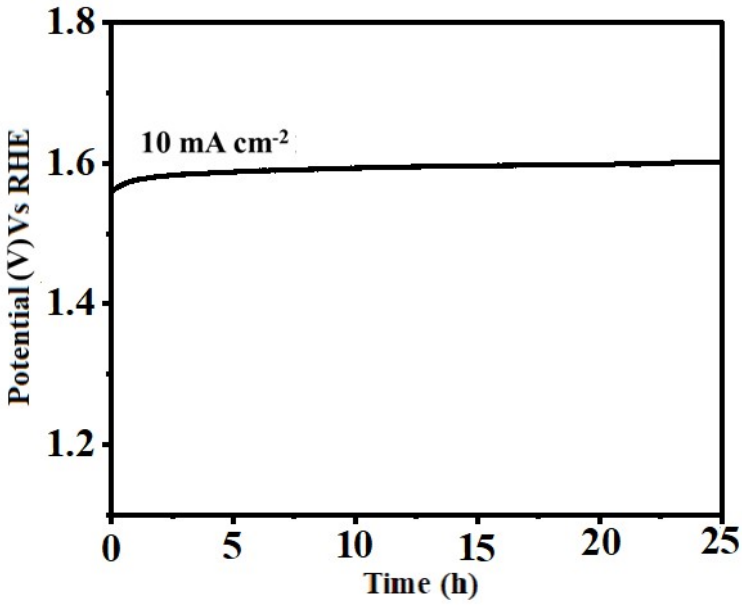

**Figure S20. Digital photographs of the colorimetric test for confirmation of oxidizing chlorine species: a) alkaline seawater after long-term stability of OER; b) 0.5 M NaClO solution (positive control)**

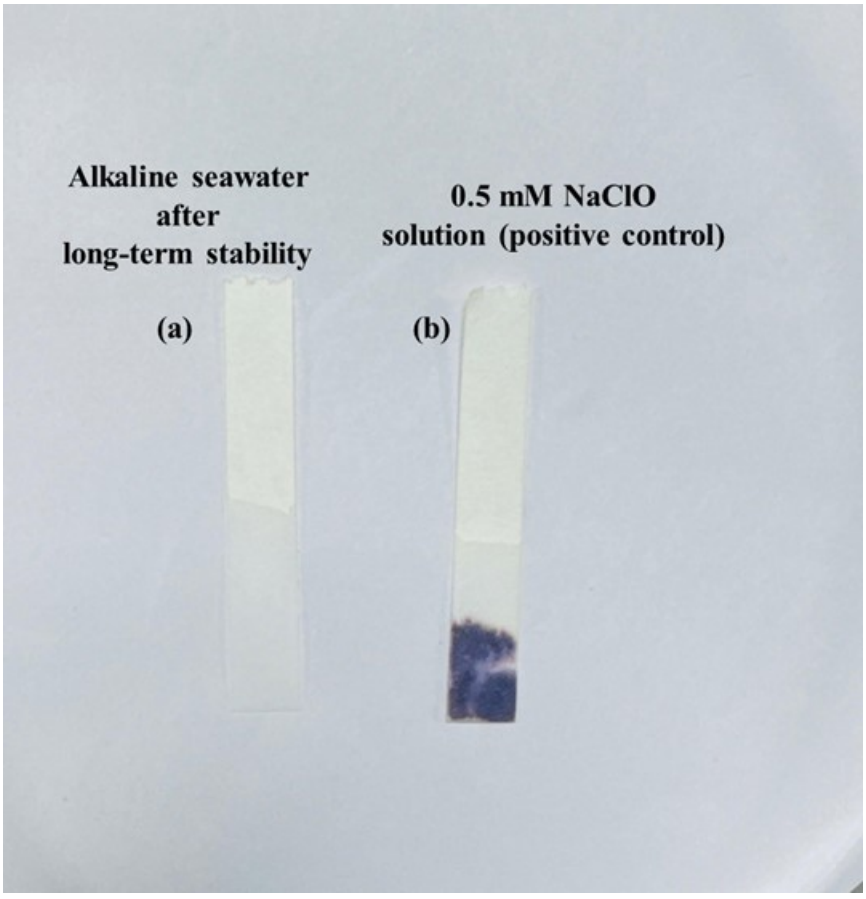

**Figure S21. Full cell chronopotentiometry of N@C-$Ni_{1.2}$-$Fe_{0.5}$ in 1 M KOH + natural seawater**

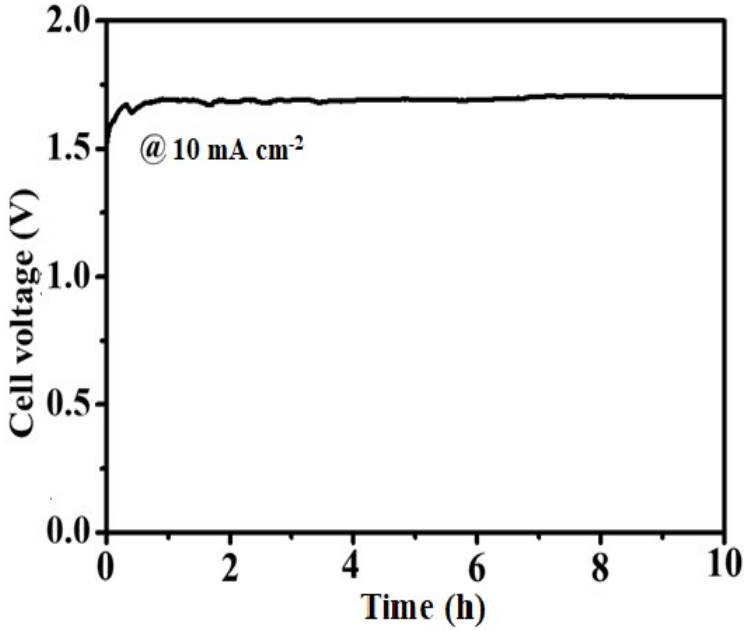

**Figure S22. Solar energy-powered water electrolyzer for hydrogen production of N@C-$Ni_{1.2}$-$Fe_{0.5}$ in 1 M KOH and alkaline seawater.**

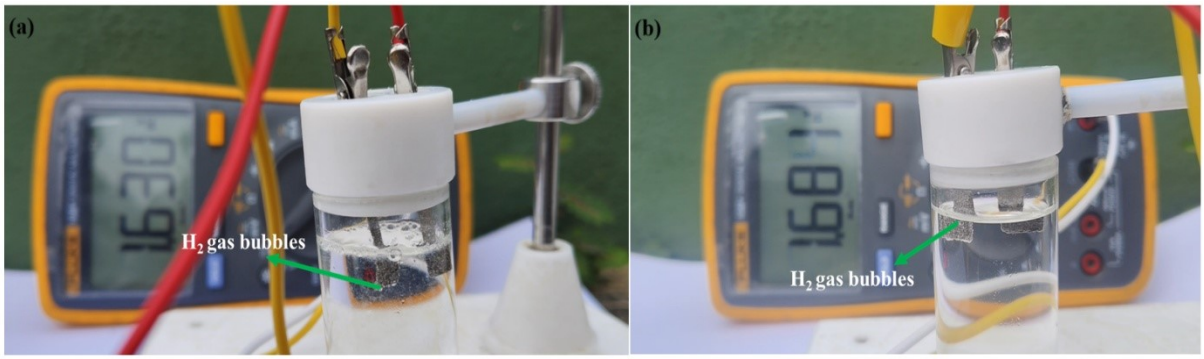

**Figure S23. Real-time demonstration of green hydrogen to electric energy by integrating the solar energy to water electrolyzer and fuel cell into a fan equipped with DC motor.**

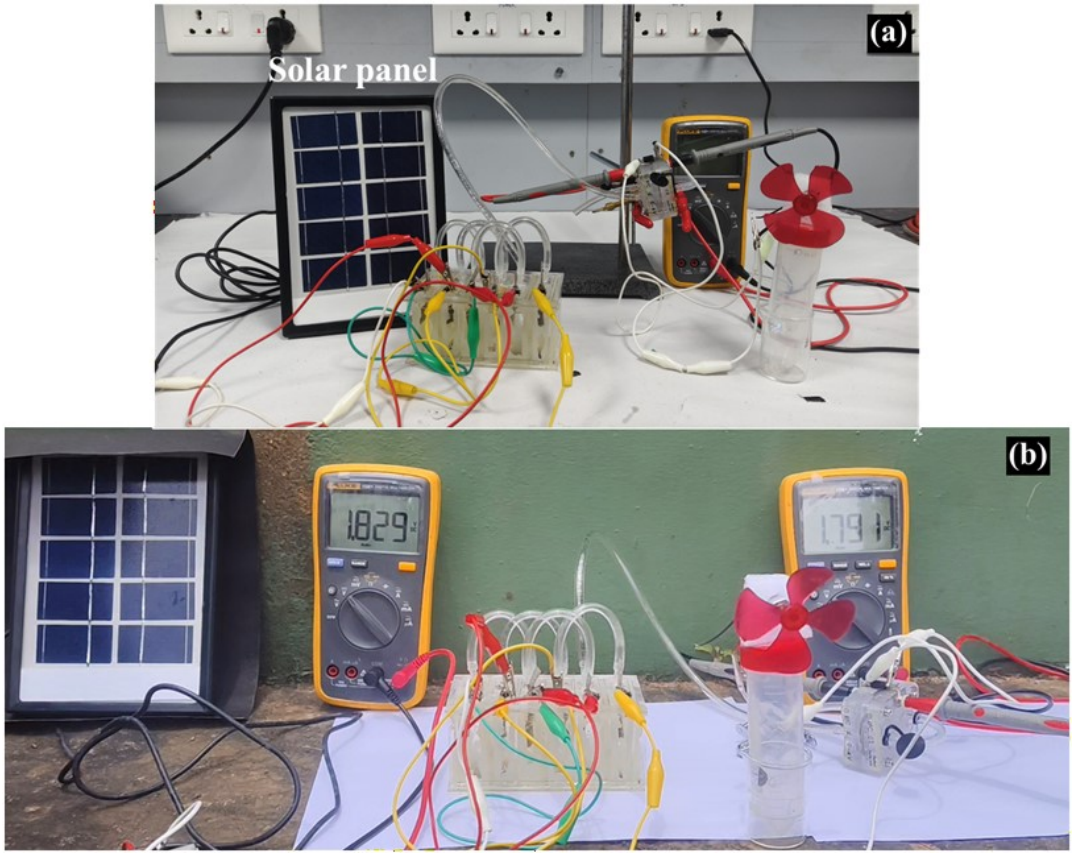


**Table S1. Obtained onset potential, oxidation peak potential and oxidation peak area of the synthesised electrocatalysts.**

| Electrocatalysts | Surface area $[m^2g^1]$ | Total Pore Volume $[cm^{-2}\ g^{-1}]$ |
|---|---|---|
| **N@C-Ni$_1$-Fe$_{0.5}$** | 8.57 | 0.0312 |
| **N@C-Ni$_{1.2}$-Fe$_{0.5}$** | 11.81 | 0.0381 |
| **N@C-Ni$_{1.4}$-Fe$_{0.5}$** | 7.92 | 0.0251 |

**Table S2. Obtained oxidation peak potential and oxidation peak area of the synthesised electrocatalysts.**

| Electrocatalysts | Oxidation peak potential (V) | Oxidation peak area ($mC/cm^2$) |
|---|---|---|
| **N@C-$Ni_1$-$Fe_{0.5}$** | 1.506 | 0.677 |
| **N@C-$Ni_{1.2}$-$Fe_{0.5}$** | 1.507 | 0.726 |
| **N@C-$Ni_{1.4}$-$Fe_{0.5}$** | 1.48 | 0.431 |
| **NF** | 1.402 | 0.0126 |

**Table S3. Charge transfer co-efficient (α) values of synthesized electrocatalysts for OER.**

| Electrocatalysts | Charge transfer co-efficient |
|---|---|
| N@C-$Ni_1$-$Fe_{0.5}$ | 0.266 |
| N@C-$Ni_{1.2}$-$Fe_{0.5}$ | 0.36 |
| N@C-$Ni_{1.4}$-$Fe_{0.5}$ | 0.26 |
| $IrO_2$ | 0.264 |
| $RuO_2$ | 0.31 |
| PPY | 0.2 |
| N@C-$Fe_2O_3$ | 0.25 |
| NF | 0.064 |

**Table S4. OER turnover frequency values of electrocatalysts.**

| Electrocatalysts | Turn over frequency ($s^{-1}$) |
|---|---|
| N@C-$Ni_1$-$Fe_{0.5}$ | 0.0067 |
| N@C-$Ni_{1.2}$-$Fe_{0.5}$ | 0.0177 |
| N@C-$Ni_{1.4}$-$Fe_{0.5}$ | 0.0025 |
| $IrO_2$ | 0.0036 |
| $RuO_2$ | 0.0059 |
| PPY | 0.0007 |
| N@C-$Fe_2O_3$ | 0.0012 |

**Table S5. EIS equivalent circuit parameters for fitting the Nyquist plots of different catalysts in 1M KOH towards the OER region.**

| Catalyst | Rs (Ω) | CPE1 (S·sn) | Rp (Ω) | CPE2 (S·sn) | Rct (Ω) |
|---|---|---|---|---|---|
| N@C-$Ni_1$-$Fe_{0.5}$ | 7.968 | 0.004364 | 1.477 | 0.01503 | 6.228 |
| N@C-$Ni_{1.2}$-$Fe_{0.5}$ | 6.316 | 0.0004606 | 0.3599 | 0.0157 | 4.601 |
| N@C-$Ni_{1.4}$-$Fe_{0.5}$ | 7.841 | 0.005461 | 1.528 | 0.01707 | 9.416 |
| Ni-Fe oxide | 2.415 | 0.1115 | 13.5 | 0.05135 | 14.38 |

**Table S6. Comparison of OER performance of N@C-$Ni_{1.2}$-$Fe_{0.5}$ with recently reported transition metal-based electrocatalysts.**

| Electrocatalyst | Support | Electrolyte | Over potential (mV) @10 mA $cm^{-2}$ | Ref |
|---|---|---|---|---|
| N@C-$Ni_{1.2}$-$Fe_{0.5}$ | NF | 1 M KOH | 310 | This work |
| Co@PANI | NF | 1 M KOH | 341 | [2] |
| SNCF | NF | 1 M KOH | 341 | [3] |
| CoP@NiFe LDH/Ni | NF | 1 M KOH | 351 | [4] |
| $Fe_{0.5}Ni_{0.5}$Pc-CP | NF | 1 M KOH | 317 | [5] |
| N-CoO@CoP@NF | NF | 1 M KOH | 313 | [6] |
| $NiCo_2O_4$/NF | NF | 1 M KOH | 319 | [7] |
| NiO/$NiCo_2O_4$ | NF | 1 M KOH | 336 | [8] |
| $LaCoO_3$/$NiCo_2O_4$ | NF | 1 M KOH | 353 | [9] |

| | | | | |
|---|---|---|---|---|
| V(III)-$NiCo_2O_4$ | CC | 1 M KOH | 344 | [10] |
| $NiCo_2O_4$/CoNC-NS | CC | 1 M KOH | 352 | [11] |

**Table S7. Charge transfer co-efficient (α) values of synthesised electrocatalysts for HER.**

| Electrocatalysts | Charge transfer co-efficient |
|---|---|
| N@C-$Ni_1$-$Fe_{0.5}$ | 0.55 |
| N@C-$Ni_{1.2}$-$Fe_{0.5}$ | 0.6 |
| N@C-$Ni_{1.4}$-$Fe_{0.5}$ | 0.54 |
| Pt/C | 0.75 |
| PPY | 0.29 |
| N@C-$Fe_2O_3$ | 0.5 |
| NF | 0.13 |

**Table S8. HER turnover frequency values of electrocatalysts.**

| Electrocatalysts | Turn over frequency ($s^{-1}$) |
|---|---|
| N@C-$Ni_1$-$Fe_{0.5}$ | 0.0438 |
| N@C-$Ni_{1.2}$-$Fe_{0.5}$ | 0.0498 |
| N@C-$Ni_{1.4}$-$Fe_{0.5}$ | 0.0393 |
| Pt/C | 0.0544 |
| PPY | 0.0248 |
| N@C-$Fe_2O_3$ | 0.0048 |

**Table S9. EIS equivalent circuit parameters for fitting the Nyquist plots of different catalysts in 1M KOH towards the HER region.**

| Catalyst | Rs (Ω) | CPE1 (S·sn) | Rp (Ω) | CPE2 (S·sn) | Rct (Ω) |
|---|---|---|---|---|---|
| N@C-$Ni_1$-$Fe_{0.5}$ | 3.572 | 0.01457 | 1.214 | 0.03162 | 14.95 |
| N@C-$Ni_{1.2}$-$Fe_{0.5}$ | 2.129 | 4.184E-5 | 2.291 | 0.0001183 | 5.75 |
| N@C-$Ni_{1.4}$-$Fe_{0.5}$ | 2.103 | 4.523E-5 | 2.457 | 0.0001883 | 15.34 |
| Ni-Fe oxide | 3.404 | 0.000402 | 7.586 | 0.0001903 | 16.5 |

| **Electrocatalyst** | **Electrolyte** | **Over potential (mV) @10 mA cm$^{-2}$** | **Substrate** | **Ref.** |
|---|---|---|---|---|
| N@C-$Ni_{1.2}$-$Fe_{0.5}$ | 1.0 M | 104 | NF | This work |
| SCSCO6 | 1.0 M KOH | 174 | NF | [12] |

**Table S10. Comparison of HER performance of N@C-$Ni_{1.2}$-$Fe_{0.5}$ with recently reported transition metal-based electrocatalysts.**

| | | | | |
|---|---|---|---|---|
| $Co(OH)_2$ | 1.0 M KOH | 182 | NF | [13] |
| $NiFe_2O_4$/NiFe LDH | 1.0 M KOH | 130 | NF | [14] |
| CoP | 1.0 M KOH | 130 | NF | [15] |
| $NiFe_xP$@NiCo-LDH | 1.0 M KOH | 140 | NF | [16] |
| $FeCoS_2/Co_4S_3$ | 1.0 M KOH | 172 | NF | [17] |
| $Ni_3S_2$/NiFe-LDH-5 | 1.0 M KOH | 135 | NF | [18] |
| CoP@Ni/Fe−P | 1.0 M KOH | 125 | CC | [19] |
| $CoMoO_4$−CoP | 1.0 M KOH | 122 | NC | [20] |
| CoP@$MoS_2$ | 1.0 M KOH | 119 | NF | [21] |

**Table S11. Comparison of overall water splitting performance of N@C-$Ni_{1.2}$-$Fe_{0.5}$ with recently reported transition metal-based electrocatalysts.**

| **Electrocatalyst** | **Electrolyte (KOH)** | **Over potential @10 mA $cm^{-2}$** | **Substrate** | **Ref.** |
|---|---|---|---|---|
| N@C-$Ni_{1.2}$-$Fe_{0.5}$ | 1.0 M | 1.63 V | NF | This work |
| $Co(OH)_2$@NCNTs@NF | 1.0 M | 1.72 V | NF | [22] |
| CP/CTs/Co-S | 1.0 M | 1.74 V | Carbon paper | [23] |

| | | | | |
|---|---|---|---|---|
| $Ni_3S_2$/NF | 1.0 M | 1.76 V | NF | [24] |
| Co-P film | 1.0 M | 1.74 V | Copper foil | [25] |
| Co-Fe Composite film | 1.0 M | 1.68 V | Carbon paper | [26] |
| NiCo alloy | 1.0 M | 1.68 V | NF | [27] |
| CoP/PNC | 1.0 M | 1.68 V | PNC | [28] |
| SCSCO6 | 1.0 M | 1.64 V | NF | [12] |
| $Co(OH)_2$ | 1.0 M | 1.66 V | NF | [13] |
| $NiFe_2O_4$/VACNT | 1.0 M | 1.72 V | VACNT | [29] |
| Ni-P film | 1.0 M | 1.67 V | Copper foil | [30] |
| PO-Ni/Ni-N-CNFs | 1.0 M | 1.69 V | CFP | [31] |
| Cop/MoP@NC/CC | 1.0 M | 1.71 V | CC | [32] |
| NiFe/$NiCo_2O_4$/NF | 1.0 M | 1.67 V | NF | [33] |
| $NiCo_2O_4$ | 1.0 M | 1.65 **V** | NF | [34] |

**Reference**


1 C. C. L. McCrory, S. Jung, I. M. Ferrer, S. M. Chatman, J. C. Peters and T. F. Jaramillo, *J. Am. Chem. Soc.*, 2015, **137**, 4347–4357.

2 S. Sriram, S. Mathi, B. Vishnu, B. Karthikeyan and J. Jayabharathi, *ChemistrySelect*, 2022, **7**, e202104516.

3 R. Hu, M. Zhao, H. Miao, F. Liu, J. Zou, C. Zhang, Q. Wang, Z. Tian, Q. Zhang and J. Yuan, *Nanoscale*, 2022, **14**, 10118–10124.

4 T. Liu, X. Yu, S. Yu, H. Yang, Q. Sun, C. Wang, S. Li and J. Y. Zheng, *J. Alloys Compd.*, 2024, **973**, 172886.

5 D. Qi, X. Chen, W. Liu, C. Liu, W. Liu, K. Wang and J. Jiang, *Inorg. Chem. Front.*, 2020, **7**, 642–646.

6 A. Vazhayil, L. Vazhayal, S. Ashok C, J. Thomas and N. Thomas, *ChemCatChem*, **16**, p.e202301250.

7 W. Bao, Y. Li, J. Zhang, T. Ai, C. Yang and L. Feng, *Int. J. Hydrogen Energy*, 2023, **48**, 12176–12184.

8 P. Li, Y. Wang, X. Du and X. Zhang, *Int. J. Hydrogen Energy*, 2023, **48**, 34783–34793.

9 G. Liu, Y. Cheng, M. Qiu, C. Li, A. Bao, Z. Sun, C. Yang and D. Liu, *J. Colloid Interface Sci.*, 2023, **643**, 214–222.

10 M. Yan, Y. Zeng, Y. Mou, J. Hu, W. Tang, C. Jiang, Q. Li and Y. Zhao, *J. Alloys Compd.*, 2023, **931**, 167465.

11 Z. Zhu, J. Zhang, X. Peng, Y. Liu, T. Cen, Z. Ye and D. Yuan, *Energy & Fuels*, 2021, **35**, 4550–4558.

12 S. Sriram, B. Vishnu and J. Jayabharathi, *ChemistrySelect*, 2023, **8**, e202301402.

13 S. Sriram, S. Mathi, B. Vishnu and J. Jayabharathi, *Energy and Fuels*, 2022, **36**, 7006–7016.

14 X. Zhang, Y. Qiu, Q. Li, F. Liu, X. Ji and J. Liu, *Int. J. Hydrogen Energy*, 2022, **47**, 40826–40834.

15 J. Zheng, A. Wu, H. Chen, X. Lv, A. Xu and X. Li, *Int. J. Hydrogen Energy*, 2021, **46**, 2026–2035.

16 W. He, S. Wu, Z. Zhang, P. Duan and Q. Yang, *Int. J. Hydrogen Energy*, 2024, **51**, 44–54.

17 S. Wang, X. He, S. Wang, X. Huang, M. Wu and D. Xiang, *Electrochim. Acta*, 2023, **441**, 141790.

18 M. R. Kumar, D. Thiruvengadam, A. Davidrichetson, J. Jayabharathi and M. Padmavathy, *ACS Appl. Mater. Interfaces*, 2025, **17**, 54926–54942.

19 L. Yu, P. Wu, T. Tian, X. He, M. Fan and L. Cui, *Dalton Transactions*, 2023, **52**, 11941–11948.

20 J. Luo, Y. Zhou, X. Wang, Y. Gu, W. Liu, S. Wang and J. Zhang, *J. Colloid Interface Sci.*, 2023, **648**, 90–101.

21 T. Xia, L. Zhou, S. Gu, H. Gao, X. Ren, S. Li, R. Wang and H. Guo, *Mater. Des.*, 2021, **211**, 110165.

22 P. Guo, J. Wu, X. B. Li, J. Luo, W. M. Lau, H. Liu, X. L. Sun and L. M. Liu, *Nano Energy*, 2018, **47**, 96–104.

23 J. Wang, H. X. Zhong, Z. L. Wang, F. L. Meng and X. B. Zhang, *ACS Nano*, 2016, **10**, 2342–2348.

24 L. L. Feng, G. Yu, Y. Wu, G. D. Li, H. Li, Y. Sun, T. Asefa, W. Chen and X. Zou, *J. Am. Chem. Soc.*, 2015, **137**, 14023–14026.

25 N. Jiang, B. You, M. Sheng and Y. Sun, *Angewandte Chemie*, 2015, **127**, 6349–6352.

26 W. Liu, K. Du, L. Liu, J. Zhang, Z. Zhu, Y. Shao and M. Li, *Nano Energy*, 2017, **38**, 576–584.

27 B. Zhang, X. Zhang, Y. Wei, L. Xia, C. Pi, H. Song, Y. Zheng, B. Gao, J. Fu and P. K. Chu, *J. Alloys Compd.*, 2019, **797**, 1216–1223.

28 Z. Peng, Y. Yu, D. Jiang, Y. Wu, B. Y. Xia and Z. Dong, *Carbon N. Y.*, 2019, **144**, 464–471.

29 Y. Xu, Y. Yan, T. He, K. Zhan, J. Yang, B. Zhao, K. Qi and B. Y. Xia, *Carbon N. Y.*, 2019, **145**, 201–208.

30 N. Jiang, B. You, M. Sheng and Y. Sun, *ChemCatChem*, 2016, **8**, 106–112.

31 Z. Y. Wu, W. B. Ji, B. C. Hu, H. W. Liang, X. X. Xu, Z. L. Yu, B. Y. Li and S. H. Yu, *Nano Energy*, 2018, **51**, 286–293.

32 Y. J. Tang, H. J. Zhu, L. Z. Dong, A. M. Zhang, S. L. Li, J. Liu and Y. Q. Lan, *Appl. Catal. B*, 2019, **245**, 528–535.

33 C. Xiao, Y. Li, X. Lu and C. Zhao, *Adv. Funct. Mater.*, 2016, **26**, 3515–3523.

34 X. Gao, H. Zhang, Q. Li, X. Yu, Z. Hong, X. Zhang, C. Liang and Z. Lin, *Angew. Chem. Int. Ed.*, 2016, **55**, 6290–6294.